

Influence of the threading dislocations on the electrical properties in epitaxial ZnO thin films

W.-R. Liu^a, W.F. Hsieh^a, C.-H. Hsu^b, K.S. Liang^b, F.S.-S. Chien^{c,*}

^aDepartment of Photonics and Institute of Electro-optical Engineering, National Chiao Tung University, Hsinchu 300, Taiwan

^bNational Synchrotron Radiation Research Center, Hsinchu 300, Taiwan

^cDepartment of Physics, Tunghai University, Taichung 407, Taiwan

Received 18 May 2006; received in revised form 5 September 2006; accepted 21 September 2006

Communicated by M. Kawasaki

Available online 28 November 2006

Abstract

The structural and electrical properties of epitaxial ZnO films grown by pulsed-laser deposition on sapphire (0001) were investigated by high-resolution X-ray diffraction (XRD), atomic force microscopy (AFM), scanning capacitance microscopy (SCM), conductive atomic force microscopy (C-AFM), and transmission electron microscopy (TEM). The results of XRD and AFM revealed that the ZnO films have a columnar-grain structure consisting of epitaxial cores surrounded by annular boundaries. The core and boundary regions exhibited significantly different capacitive responses and field emission current. The results of TEM indicated that the annular boundaries have high-density edge threading dislocations. The shift of flatband voltage and the raise of potential barrier at the boundaries observed by SCM and C-AFM were attributed to the interface trap densities caused by the existence of high-density edge threading dislocations. © 2006 Elsevier B.V. All rights reserved.

PACS: 61.10.Nz; 61.72.Ff; 68.37.Vj; 68.55.Jk

Keywords: A1. Defects; A1. Surfaces; A3. Laser epitaxy; B1. Oxides; B2. Semiconducting II–VI materials

1. Introduction

Wurtzite-structure ZnO is a II–VI semiconductor with a wide direct band gap of 3.37 eV. One of the most attractive features of ZnO is the large exciton binding energy of 60 meV, which is almost three times higher than that of GaN (25 meV) [1]. Therefore, ZnO is considered as an excellent candidate for UV and blue lasers with low thresholds at high temperatures. Recently, Tsukazaki et al. [2] demonstrated the first blue light-emitting diode (LED) based on ZnO material using laser molecular beam epitaxy. The most important issue for the growth of high-quality ZnO film is to diminish the strain of hetero-epitaxial layers. With regard to ZnO films grown on (0001) sapphire, reflection high-energy electron diffraction (RHEED) measurements exhibit that the [10 $\bar{1}$ 0] direction

of the ZnO epilayer is rotated by 30° with respect to that of the underneath (0001) sapphire substrate, so that the lattice mismatch is reduced from 32 to 18% [3]. The strain energy, introduced by such a large lattice mismatch, has to be released by means of various defects in the epitaxial film. The characteristic defects of ZnO epitaxial films investigated by the transmission electron microscopy (TEM) are high-density threading dislocations (TDs) (typically 10⁹–10¹¹ cm⁻²) apparently passing through entire films [4,5]. As reported in many studies in GaN epitaxial films, TDs can influence the electrical and optical properties of films, including the degradation of devices through carrier scattering [6], nonradiative recombination [7], and reverse-bias leakage current [8,9]. ZnO has the same crystal structure as GaN, both belonging to space group P6_{3mc}. However, in ZnO thin films, very few studies have discussed the influence of TDs on electrical properties so far.

Scanning probe microscopy (SPM) has been employed to characterize the local electrical properties in

*Corresponding author. Tel.: +8864 23590121 2407.

E-mail address: fsschien@thu.edu.tw (F.S.-S. Chien).

semiconductor materials. Varied from SPM, scanning capacitance microscopy (SCM) and conductive atomic force microscopy (C-AFM) are applied to measure the distribution of dislocation near the surface. SCM offers the information of charge carriers of semiconductors in response to a low-frequency ac electrical modulation between the sample and the tip [10]. The SCM signal is detected as the capacitance between the sample and the tip with a resonance capacitance sensor, and the SCM images are constructed from the two dimensional dC/dV signals, which represent the slope of the capacitance (C)–voltage (V) curve at a certain dc tip bias (V_{tip}). In addition, the dC/dV versus V_{tip} curve collected at a fixed position provides the information of local carrier properties. As for C-AFM, a metallized SPM probe contacts the sample to serve as a microscopic Schottky contact. The current (I) is detected and amplified as a bias voltage (V) is applied to the probe. The images of sample topography and current leakage can be simultaneously acquired [8].

In this study, we applied SPM, X-ray diffraction (XRD), and TEM to characterize the correlation between electrical properties and TDs in the epitaxial ZnO films. The results of XRD and AFM topography reveal that the ZnO film has a columnar-grain structure, which consists of epitaxial cores and annular boundary. The TEM result indicates high-density edge TDs inhered in the annular boundary. Furthermore, the SCM and C-AFM measurements suggest that the edge TDs induce interface trap density, which accounts for the flatband voltage shifts and the potential barrier increases at the boundary.

2. Experiments

The ZnO films were grown on a (0001) sapphire substrate by pulsed-laser deposition (PLD), which is popularly adapted for growing ZnO epi-films [2,11]. A KrF excimer laser ($\lambda = 248$ nm) was employed and the beam was focused to produce an energy density of $\sim 5\text{--}7$ J cm $^{-2}$ at 10 Hz repetition rate on a commercial hot pressed stoichiometric ZnO (99.99% purity) target. The films were deposited at a growth rate of ~ 0.625 Å s $^{-1}$ at 600 °C substrate temperature and a base vacuum of 3.5×10^{-9} Torr, followed by in-situ annealing at 700 °C for 1 h. No oxygen gas flow was introduced during the process of growth and annealing. Hall measurements yielded a background electron concentration of 2.87×10^{17} – 7.06×10^{18} cm $^{-3}$ with the mobility of 28.2–40.9 cm 2 V $^{-1}$ s $^{-1}$ and the resistivity of 0.771–0.0216 Ω cm using the Van der Pauw configuration (Bio-Rad Microscience HL5500 Hall System) at room temperature.

The high-resolution XRD analysis was conducted at beamline BL17 of National Synchrotron Radiation Research Center (NSRRC) with incident X-ray wavelength of 1.3332 Å. The photoluminescence (PL) measurement was carried out with wavelength of 325 nm He–Cd laser, and the light emission was collected into a Triax 320 spectrometer. The SCM and C-AFM were carried out with a

commercial closed-loop-scanner SPM (Digital Instruments 3100) with Ti/Pt-coated cantilevers (MikroMasch). Finally, the TEM measurement was performed by a Philips TECNAI-20 FEG operated at 200 kV.

3. Results and discussion

Fig. 1(a) shows the azimuthal scan across ZnO $\{20\bar{2}1\}$ diffraction peaks. The existence of 6 sharp peaks with 60° interval verifies that the ZnO film is epitaxially grown on the sapphire substrate. The XRD radial scans across the surface normal (0002) and in-plane (10 $\bar{1}$ 0) reflections (to be reported elsewhere) reveal that the lattice parameters of ZnO are $a = 3.238$ Å and $c = 5.225$ Å. These values illustrate that the ZnO epitaxial films experience a tensile strain (0.338%) in the growth direction and a compressive strain (0.365%) in the lateral direction, which agree well with the results reported in the study of ZnO films [12]. The full-width at half-maximum (FWHM) of the ω -rocking curve of the (0002) reflection is 0.057°, indicating the presence of a the small mosaicity along surface normal.

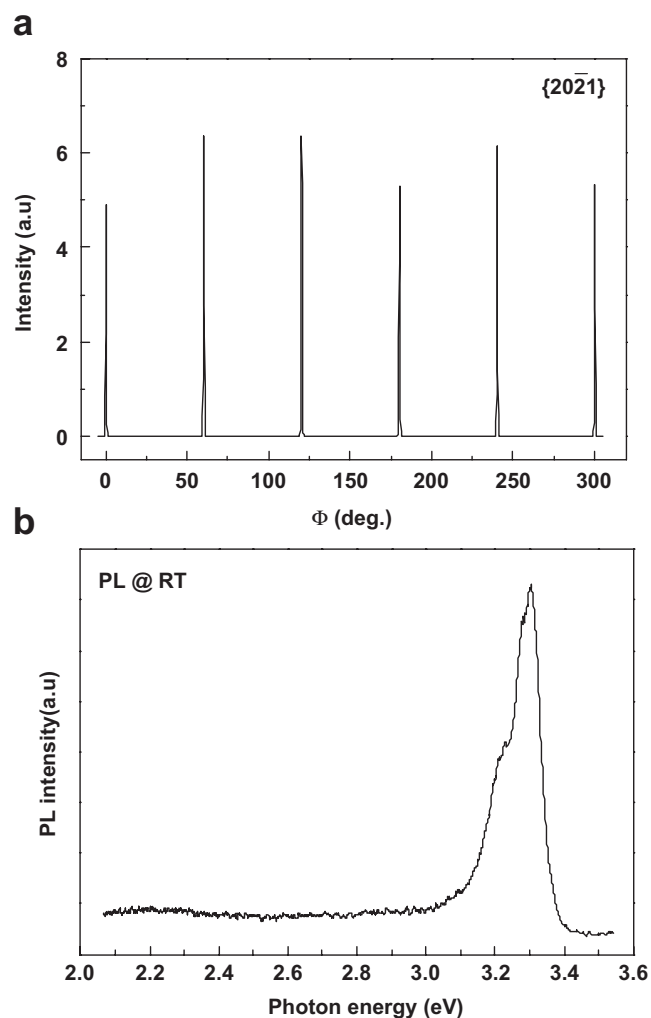


Fig. 1. The azimuthal scan of the ZnO $\{20\bar{2}1\}$ X-ray diffracted peak (a) and PL spectrum measured at room temperature (b).

The in-plane structural coherence length along $[10\bar{1}0]$ direction, estimated from the line width of in-plane radial scan using the Scherrer formula, is ~ 100 nm. These XRD results reveal that the ZnO film is epitaxially grown on (0001) sapphire and consists of grains of ~ 100 nm diameter in the lateral direction. Fig. 1(b) shows that the PL near band emission is about 3.28 eV with FWHM of 105 meV. No defect emission was observed at the visible region, ensuring a good structural quality of the ZnO films.

Fig. 2(a) and (b) show the AFM topography and the SCM images simultaneously acquired while the tip was applied with a V_{tip} of 0.664 V plus a 2 V ac modulation at 23 kHz. Viewing the topographic image, we observed small grains of 80–110 nm in diameter, which is comparable to the grain size obtained by XRD. We thus propose that the ZnO film has a columnar-grain structure consisting of epitaxial core and annular boundary. The bright and dark regions in the topographic AFM image are associated with the epitaxial cores and the boundaries, respectively.

The correlation between the AFM and the SCM images is obvious. It is worth noting that we exclude the correlation is due to topographic effect on the capacitance signals since the root-mean-square surface roughness is only 1.2 nm and the SCM contrast vanishes as a negative V_{tip} is applied. The $dC/dV-V_{\text{tip}}$ curves shown in Fig. 2(c) were extracted from the grain region (cross marked A) and from the boundary region (cross marked B) in Fig. 2(b), respectively. The curves were obtained after averaging forward and reverse sweeps to exclude the piezoelectricity of ZnO. It was found that the peak value of dC/dV signal at point A is lower than that at point B, implying that the grain region has the capacitance with less dependence on the dc bias and its local free carrier concentration in the grain region is higher than that at the boundary. The flatband voltage, defined as the voltage at the dC/dV peak, shifts about +0.57 V between the two regions; this accounts for the SCM contrast at the optimum V_{tip} (0.664 V). Furthermore, the coincidence of the curves as

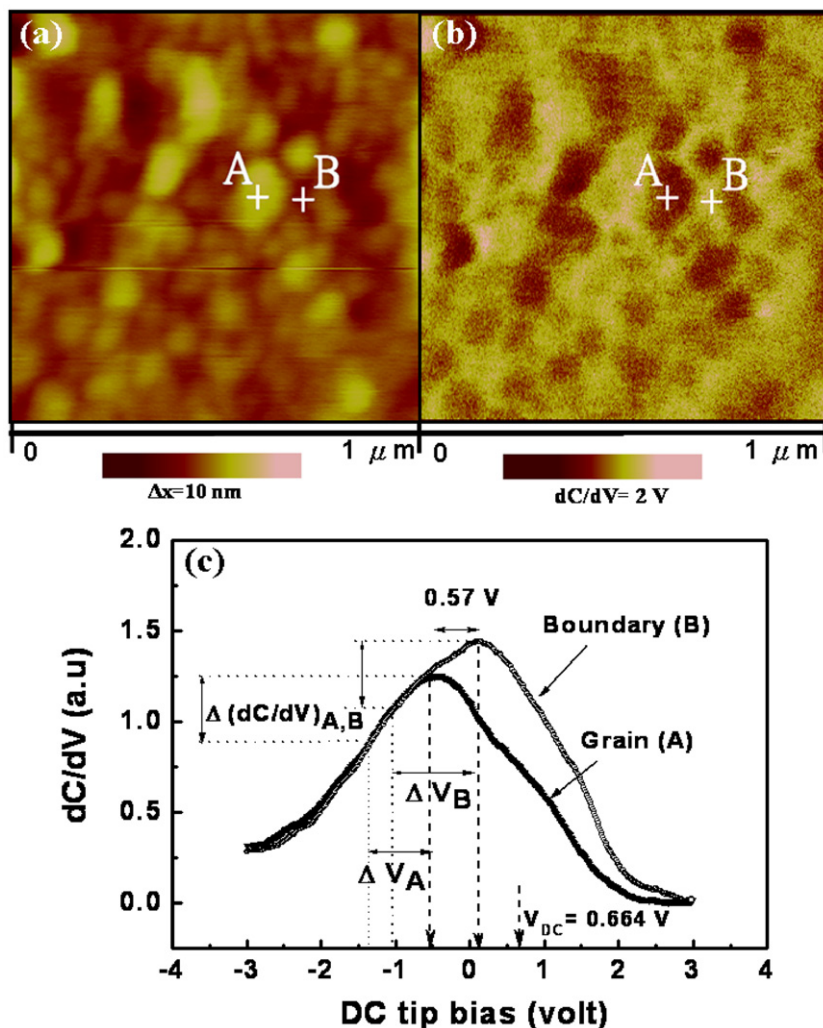


Fig. 2. AFM topography (a) and SCM differential capacitance (dC/dV) image (b) acquired at $V_{\text{tip}} = 0.664$ V in ZnO film. Local $dC/dV-V_{\text{tip}}$ curve measured on the grain (cross marked A) and at the boundary (cross marked B) as a function of V_{tip} are shown in (c). ΔV_A and ΔV_B represent the variation of V_{tip} with the same change in $(dC/dV)_{A,B}$ (or surface potential). The dash lines show the dC/dV peaks (flatband voltage) of the curves.

the V_{tip} set below -0.7 V suggests that the response of charge carriers to ac modulation is similar between the post-depletion and the inversion realms.

The shift of flatband voltage can be attributed to two factors: interface trap density (D_{it}) and fixed charge density (N_f) [13]. N_f only causes a shift of dC/dV curve, but D_{it} can introduce not only a shift but also a stretch. Hong et al. [14] reported that the ratio of FWHM of dC/dV curve to ΔV is fixed only if D_{it} is present, where ΔV represents the deviation in bias from the dC/dV peak with a given change in dC/dV value (and hence a change in surface potential). The ratios of FWHM to ΔV in the grain and boundary regions estimated from Fig. 2(c) are 0.85 and 0.91, respectively. Consequently, we believe that the shift of flatband voltage is mainly caused by the effect of D_{it} , which is higher in boundary regions than in the grain regions. Accordingly, the local carrier concentration should be lower at the boundary region, which agrees with the inference from the peak value of dC/dV above.

Fig. 3(a) and (b) show the AFM topography and current images simultaneously extracted under $V_{\text{tip}} = 3\text{ V}$, with the current image shown at reverse contrast. To manifest the correlation between topography and conductivity, these two images are overlaid as shown in Fig. 3(c). The current spots, indicative of the more conductive regions, occur only in the grains but not at the boundaries. The I - V curves

taken in the grain (cross marked A) and at the boundaries (cross marked B) are both shown in Fig. 3(d). The observed shift of forward bias between grain and boundary indicates the possibility of charge trapping. The current apparently diminishes at the reverse bias because of the rectification of the nonideal Pt/ZnO Schottky contact, as there exists a native insulator at the tip-sample junction. In addition, the emission current at the boundary is lower than that at the grain, reflecting that the boundary has a potential barrier higher than the grain.

The defect nature of the TD in the ZnO film was characterized by the cross-sectional bright-field TEM images in two-beam contrast condition with diffraction vectors $\mathbf{g} = (11\bar{2}0)$ in Fig. 4(a) and $\mathbf{g} = (0002)$, in Fig. 4(b). Many TDs with $[0001]$ direction are visible. Three categories of TDs with a vertical $[0001]$ direction have been classified on the basis of their Burgers vector (\mathbf{b}) in hexagonal structures [4,5], namely edge dislocation ($\mathbf{b}_E = 1/3\langle 11\bar{2}0 \rangle$), screw dislocation ($\mathbf{b}_C = \langle 0001 \rangle$), and mixed dislocation ($\mathbf{b} = 1/3\langle 11\bar{2}3 \rangle$). According to the invisibility criterion (i.e., $\mathbf{g} \cdot \mathbf{b} = 0$), the pure screw and edge TDs are invisible in the images taken with the \mathbf{g} vector along $(11\bar{2}0)$ and (0002) , respectively.

The edge, screw, and mixed TDs densities are about $1.6 \times 10^{10}\text{ cm}^{-2}$, $2.5 \times 10^8\text{ cm}^{-2}$ and $6.9 \times 10^8\text{ cm}^{-2}$ as respectively estimated from Fig. 4(a) and (b). The diversity

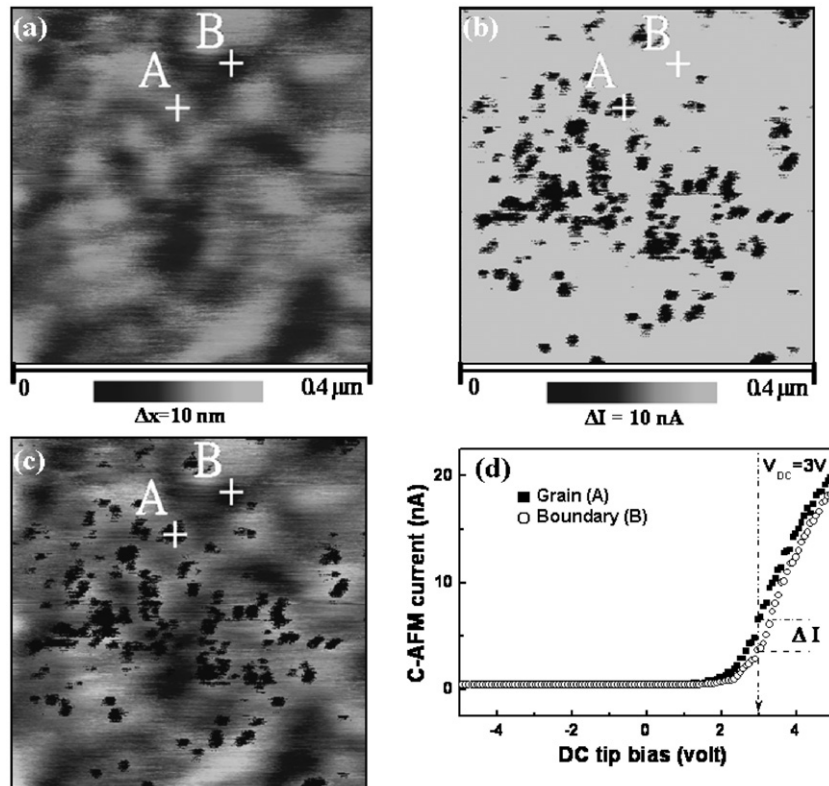


Fig. 3. AFM topography (a) and C-AFM current image (b) of ZnO film with area of $0.4 \times 0.4\ \mu\text{m}^2$ acquired at $V_{\text{tip}} = 3\text{ V}$. The current image was shown at reverse contrast. Overlaid images of (a) and (b) with the same area was shown in (c). Local I - V_{tip} curves taken in the bright region (cross marked A) and the dark region (cross marked B) of (a) as a function of V_{tip} was plotted in (d). The ΔI marks the current difference of the I - V_{tip} curves between A and B at $V_{\text{tip}} = 3\text{ V}$.

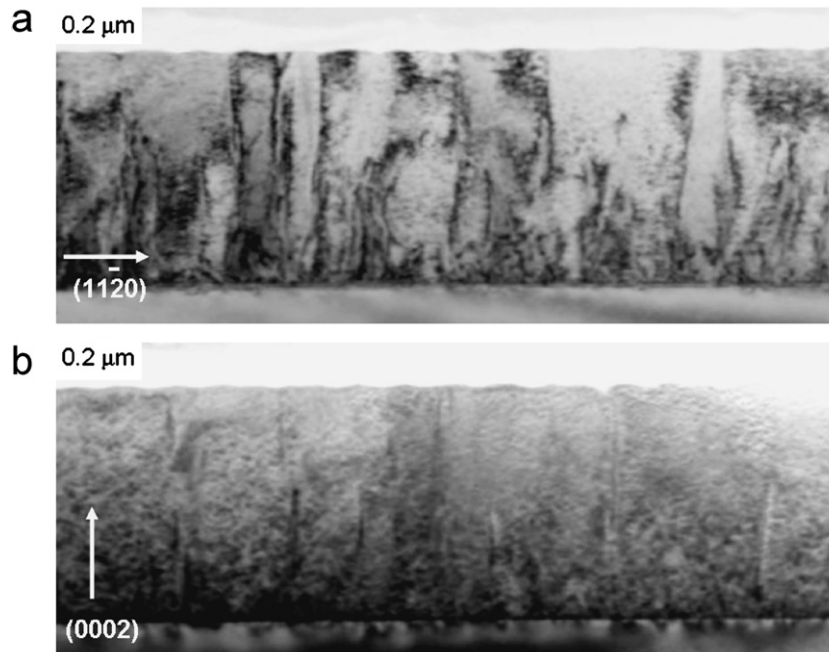


Fig. 4. Two-beam bright-field cross-sectional TEM micrographs of the ZnO film with (a) $g = (1\ 1\ \bar{2}\ 0)$ and (b) $g = (0002)$.

of dislocation densities for the three types of TDs in the ZnO thin films grown on sapphire (0001) reveal that the pure edge TDs is the major category, occupying about 94% of the total TDs. The remaining parts are the pure screw and mixed TDs type. These results agree well with other studies involving defect structure for ZnO epi-films [4,5]. Additionally, these TEM results reveal the columnar grains encompassed by the edge TDs are about 110 nm, which is well correlated with the XRD and AFM results. Also, small-angle grain boundaries were observed during the TEM measurement by tilting the sample about 0.6° , to coincide with the FWHM (0.64°) of azimuthal diffracted peak with $\{20\bar{2}1\}$, presenting another evidence that the results of TEM and XRD agree with the in-plane grain size. As alluded to the results presented above, the epitaxial core was surrounded by a small-angle grain boundary consisting of high-density edge TDs. Hence, the presence of D_{it} at the boundary would be induced by the high-density edge TDs. Tivarus et al. [15] demonstrated that the negative charge states related to the TDs close to the surface increased the local potential barrier at the dislocation, and that the emission current was suppressed at the boundary due to the increase in potential barrier associated with the negative-charged D_{it} . Consequently, the increase in the potential barrier and the charge scattering related to D_{it} would lead to the reduction of the carrier mobility, thereby degrading the performance of electro-optic devices. Therefore, the reduction of TDs is an important issue for the future application of ZnO thin films.

Although the main defect structures of epitaxial ZnO and GaN films on sapphire substrates are both edge TDs, the defect structures exhibit distinctly different influence on the electrical properties of ZnO and GaN films. For

example, the edge TDs induce negative fixed charge in GaN films [10], but generate interface trap density in ZnO films. On the other hand, because the distribution of the screw TDs is much less than that of the edge TDs, we cannot confirm the location of the screw TDs and their electrical properties.

4. Conclusions

The ZnO epitaxial films have been grown on sapphire (0001) by PLD. The local spectra of the $dC/dV-V_{tip}$ and $I-V_{tip}$ curves obtained from the SCM and C-AFM analyses suggest that the flatband voltage shifts and the potential barrier increases at the grain boundary, due to the interface trap density induced by the existence of high-density edge TDs. The ZnO epi-film on sapphire (0001) features a columnar-grain microstructure with an epitaxial core encompassed by high density of TDs at the boundary region. The principal TDs influencing the electrical properties of the ZnO epi-film are found to be of the pure edge type.

Acknowledgments

The authors thank Mr. C. M. Huang of NSRRC for his help in the X-ray diffraction measurements. We also thank the Nanotechnology Research Center, Industrial Technology Research Institute for the access of SCM and C-AFM. This work is partly supported by National Science Council (NSC) of Taiwan under grants NSC-94-2112-M-029-004, NSC-93-2112-M-009-035. One of us (W. R. Liu.) gratefully acknowledge NSC for providing a fellowship under NSC-93-2112-M-213-006.

References

- [1] Z.K. Tang, G.K.L. Wong, P. Yu, M. Kawasaki, A. Ohtomo, H. Koinuma, Y. Segawa, *Appl. Phys. Lett.* 72 (1998) 3270.
- [2] A. Tsukazaki, A. Ohtomo, T. Onuma, M. Ohtani, T. Makino, M. Sumiya, K. Ohtani, S.F. Chichibu, S. Fuke, Y. Segawa, H. Ohno, H. Koinuma, M. Kawasaki, *Nature Mater* 4 (2005) 42.
- [3] Yefan Chen, D.M. Bagnall, Hang-jun Koh, K.-T. Park, K. Hiraga, Z. Zhu, Takafumi Yao, *J. Appl. Phys.* 84 (1998) 3912.
- [4] F. Vigué, P. Vennéguès, S. Vézian, M. Lau gt, J.-P. Faürie, *Appl. Phys. Lett.* 79 (2001) 194.
- [5] S.H. Lim, J. Washburn, Z. Liliental-Weber, D. Shindo, *J. Vac. Sci. Technol. A* 19 (2001) 2601.
- [6] H.M. Ng, D. Doppalapudi, T.D. Moustakas, N.G. Weimann, Eastman, *Appl. Phys. Lett.* 73 (1998) 821.
- [7] T. Sugahara, H. Sato, M. Hao, Y. Naoi, S. Tottori, K. Yamashita, Nishino, L.T. Romano, S. Sakai, *Jpn. J. Appl. Phys. Part 2* 37 (1998) L398.
- [8] J.W.P. Hsu, M.J. Manfra, R.J. Molnar, B. Heying, J.S. Speck, *Appl. Phys. Lett.* 81 (2002) 79.
- [9] E.J. Miller, D.M. Schaadt, E.T. Yu, C. Poblenz, C. Elsass, Speck, *J. Appl. Phys.* 91 (2002) 9821.
- [10] P.J. Hansen, Y.E. Strausser, A.N. Erickson, E.J. Tarsa, P. Kozodoy, E.G. Brazel, J.P. Ibbetson, U. Mishra, V. Narayanamurti, S.P. DenBaars, J.S. Speck, *Appl. Phys. Lett.* 72 (1998) 2247.
- [11] K. Ip, Y. W Heo, D.P. Norton, S.J. Peatron, J.R. LaRoche, F. Ren, *Appl. Phys. Lett.* 85 (2004) 1169.
- [12] A.B.M.A. Ashrafi, N.T. Binh, B.P. Zhang, Y. Segawa, *Appl. Phys. Lett.* 84 (2004) 2814.
- [13] E.H. Nicollian, J.R. Brews, *MOS Physics and Technology*, Wiley, New York, 1982 ch. 10, pp. 423–491.
- [14] Y.D. Hong, Y.T. Yeow, W.K. Chim, K.M. Wong, J.J. Kopanski, *IEEE Trans. Electron. Dev.* 51 (2004) 1496.
- [15] C. Tivarus, Y. Ding, P. Pelz, *J. Appl. Phys.* 92 (2002) 6010.